Industrial Crops & Products 193 (2023) 116246

Contents lists available at ScienceDirect

Industrial Crops & Products

journal homepage: www.elsevier.com/locate/indcrop

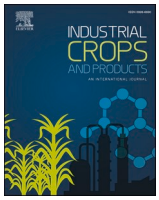

Promising nanocomposites for food packaging based on cellulose – PCL films reinforced by using ZnO nanoparticles in an ionic liquid

Elahe Amini [*,1], Cristina Valls, M. Blanca Roncero

CELBIOTECH_Paper Engineering Research Group, Universitat Politè cnica de Catalunya (UPC), BarcelonaTech, Colom 11, 08222 Terrassa, Spain

ARTICLE INFO

Keywords:
Transparent biofilm
Ring-opening polymerization
Ionic liquid
Trapping nanoparticles
Direct nanowelding

ABSTRACT

The fact that most composites consist of polluting synthetic materials has prompted a search for biodegradable replacements based on cellulose fibers and polycaprolactone as potential packaging materials. In this work, we developed a green, efficient approach to rendering hydrophobic polycaprolactone (PCL) compatible with hydrophilic cellulose fibers by using an ionic liquid as a nanowelding agent in the presence of zinc oxide nanoparticles (ZnONPs). Transparent biobased nanocomposite films were thus directly obtained by in situ ring-opening polymerization (ROP) of ε-caprolactone (CL) monomers onto the dissolved cellulose matrix by using the ionic liquid 1-ethyl-3-methylimidazolium acetate ([EMIM]Ac). [EMIM]Ac and ZnONPs were efficiently catalyzed ε-caprolactone ROP under mild conditions. Cellulose-grafted PCL nanocomposite films were obtained by adding variable amounts of CL and ZnONPs to the cellulose matrix. The maximum grafting of 40% was achieved by using 5wt% ZnONPs and 70% CL. FTIR spectra confirmed the presence of PCL in the nanocomposites. Also, FE-SEM revealed uniform dispersion of ZnONPs and PCL in the regenerated cellulose matrix, and trapping of nanoparticles in nanofibrils after the cellulose matrix was regenerated. X-ray diffraction (XRD) spectra showed a decreased apparent crystallinity and crystallite size. The XRD results also confirmed that the crystal properties of the nanocomposite films and an all-cellulose composite (ACC) were almost identical. The mechanical, barrier and optical properties of the nanocomposite films were significantly better than those of the ACC film by effect of the incorporation of ZnONPs and PCL especially with 5wt% ZnONPs and 70% CL). The nanocomposite films exhibited acceptable antioxidant activity and UV-light barrier properties, so they hold promise for used in food packaging. Nanocomposite films are in fact multifunctional materials with the potential for use in cellulose-based food packaging by virtue of their being transparent and bio-based, and possessing very good water vapor and oxygen barrier properties.

1. Introduction

Environmental concerns and sustainability issues have recently led to green materials arousing great interest. Biocomposites are often prepared by reinforcing a natural biopolymer matrix to improve specific characteristics (Rivera-Galletti et al., 2021). Cellulose is a bioorganic polymer and the most abundant polysaccharide on Earth. This polymer, which has a variety of commercial uses, consists of a large number of repeating glucose residues joined by β-1,4-glycoside linkers that allow them to adopt a tightly packed crystalline form (Amini et al., 2021). By virtue of their sustainability, low cost, flexibility and strength, biocomposites based on natural cellulose fibers have attracted renewed attention as replacements for synthetic materials and polymers. However, cellulose as such has limited use owing to its complex hydrogen-bonding network and the tight inter- and intramolecular hydrogen bonds it forms, which render it insoluble in water and common organic solvents (Gustavsson et al., 2020; Amini et al., 2021). Cellulose is dissolved by liquids such as viscose, sodium hydroxide/urea (NaOH/urea), *N*-methylmorpholine-*N*-oxide (MNO) monohydrate, *N, N*-dimethylacetamide/LiCl (DMAc/LiCl), and dimethylsulfoxide/tetrabutylammonium fluoride trihydrate (DMSO/TBAF) mixtures. These solvents, however, are hazardous, highly flammable and challenging to recover (Ichiura et al., 2017).

Novel functional cellulose-based materials with remarkable mechanical properties have been successfully created by using ionic liquids (ILs) (Zhang et al., 2017). Ionic liquids that efficiently dissolve cellulose

* Corresponding author.
E-mail address: elahe.amini@upc.edu (E. Amini).
[1] ORCID: 0000-0003-1524-0907

https://doi.org/10.1016/j.indcrop.2023.116246
Received 25 June 2022; Received in revised form 27 December 2022; Accepted 3 January 2023
Available online 10 January 2023

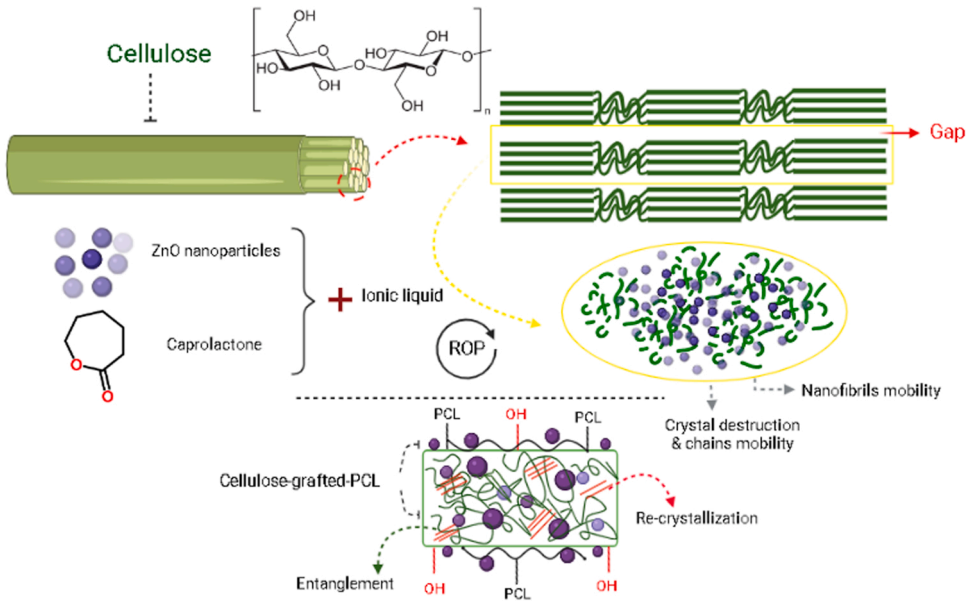

Fig. 1. Mechanism for in situ ROP of CL monomers to obtain the cellulose-grafted-PCL matrix and welding of nanofibrils with entrapped ZnONPs in [EMIM]Ac as solvent.

at room temperature by disrupting H-bonds have been deemed "green solvents" with unique physicochemical properties (Gustavsson et al., 2020 including high thermal stability, low viscosity, chemical stability, low toxicity, nonflammability and recyclability (Amini et al., 2021). The best options for dissolving cellulose appear to be ionic liquids with an aromatic imidazolium or pyridinium cation and an OAc^{-}, $HCOO^{-}$, $(MeO)^{2}PO^{2-}$, or Cl^{-} anion due to their exceptional physicochemical characteristics. ILs with dialkyl imidazolium bases, such as 1-allyl-3--methyl imidazolium chloride ([AMIM]Cl), 1-buthyl-3-methyl imidazolium chloride ([BMIM]Cl), and 1-ethyl-3-methylimidazolium acetate ([EMIM]Ac), have drawn a lot of attention to dissolve cellulose (Amini et al., 2021). Swatloski et al. (2002) succeeded in dissolving cellulose and then regenerating it by using an imidazolium-based ionic liquid (Swatloski et al., 2002). Ichiura et al. (2017) investigated the dissolution of cellulose paper in the ionic liquid 1-butyl-3-methyl-imidazollium chloride ([BMIM]Cl). Hydrogen bonds created in regenerated cellulose made the film more resistant to degradation by water than was conventionally prepared cellulose paper. If all water was removed, the recovered [BMIM]Cl was comparable in performance to virgin [BMIM]Cl. Based on reported data, 1-ethyl-3-methylimidazolium acetate ([EMIM]Ac) is a better choice for creating regenerated cellulose fiber because it has a lower dissolving temperature and requires less energy during the shaping process to form fibers with increased elongation values. Also, [EMIM]Ac residues, which can be to some extent be retained by fibers even after washing, are not toxic (Vinogradova and Chen (2016); Kosan et al., 2008). Liu et al. (2010) proved that interactions between acetate anions and hydroxyl groups of glucose are three times stronger than analogous interactions between water and hydroxyl groups. Thus, it was proven that ionic liquids may effectively dissolve H-O…H-O bonds (Liu et al., 2010; Grzabka-Zasadzińska et al., 2019).

All-cellulose composites (ACC) are self-reinforced composites where both the matrix (dissolved portion) and the reinforcement (undissolved portion) are cellulose. ACC have recently emerged as environmentally friendly alternatives based on an ecodesign concept (Chen et al., 2020a; Adak and Mukhopadhyay, 2016). Poor fiber-matrix adhesion is avoided thanks to the chemical similarity of the matrix and reinforcing phase (Chen et al., 2020a). Because cellulose is the sole component, ACC exhibit higher interfacial compatibility, lower density, total biodegradability, great mechanical properties and easy recyclability (Chen et al., 2020a; Adak and Mukhopadhyay, 2016).

Technological advancements at the micro and nanoscale have enabled the development of a wide range of structures for a variety of purposes. Nanoscale welding and joining techniques have gained much attention in this context. Joining nanotechnologies are among the clever bottom-up strategies using self-assembled materials to create next-generation nanomaterials (Amini et al., 2021; Reyes et al., 2018). Yousefi was the first to suggest using nanowelding technology to connect cellulose fibers. The crucial element in the selective dissolution procedure is the breakdown of hydrogen bonds within cellulose fibers (Moyer et al., 2018). Cellulose fibers additionally contain a variety of microdisconnections or gaps including pits and lumens that are often open and allow easy penetration of solvents. There are also other nanoscale disconnections such as those along adjoining nanofibrils (Yousefi et al., 2015; Siró and Plackett, 2010). With connected nanofibrils, the solvent can penetrate deeply into the cellulose, dissolve nanofibril surfaces and weld nanofibrils together after rinsing and drying (Yousefi et al., 2015).

Graft polymerization can provide an effective method for preparing ecofriendly cellulose-based materials for a wide range of uses in the future. In the grafting-from approach, polymer growth can be simply started by initiating sites on the cellulose backbone through controlled radical polymerization of monomers (Terzopoulou et al., 2018). One of the greatest advantages of this approach is the high graft density that can be obtained as a result of reactive groups easily accessing the chain ends of the growing polymers (Carlmark et al., 2012; Jiang et al., 2019). The grafting technique called "ring opening polymerization" (ROP) involves chain-growth of polymers via ring-opening of cyclic monomers. This is one of the most widely used choices because the high density of surface hydroxyl groups on cellulose (initiators) facilitates immediate polymerization of cyclic monomers (Zhu et al., 2021). Hafrén and Córdova (2005, 2007) reported the first instance of polycaprolactone ROP from a cellulose substrate without chemical treatment of the cellulose prior to grafting. They successfully grafted ε-caprolactone onto a cellulose matrix by using organic acids or amino acids as catalysts. The carbonyl group in polycaprolactone was assigned a peak at 1730 cm^{-1} in the FTIR spectrum. Ionic liquids are widely used as solvents and/or catalysts in organic reactions. However, they have scarcely been used in polymerization reactions. Leite et al. (2022) accomplished ε-caprolactone ROP by using an imidazolium-based ionic liquid without an

Table 1
%Grafting, %Grafting efficiency and %Homopolymer.

Sample	Grafting (%)	Grafting efficiency (%)	Homopolymer (%)
1% ZnO/10% CL	4.24	45.83	54.16
1% ZnO/30% CL	13.89	48.64	51.35
1% ZnO/50% CL	25.48	53.65	46.34
1% ZnO/70% CL	38.22	56.89	43.10
3% ZnO/10% CL	6.17	66.66	33.33
3% ZnO/30% CL	16.21	56.75	43.24
3% ZnO/50% CL	28.18	58.87	41.12
3% ZnO/70% CL	39.76	59.19	40.80
5% ZnO/10% CL	8.10	87.50	12.49
5% ZnO/30% CL	18.91	66.21	33.78
5% ZnO/50% CL	33.20	69.91	30.08
5% ZnO/70% CL	47.87	71.26	28.73

intentionally added alcohol as an initiator.

Polycaprolactone (PCL) is an FDA-approved biodegradable aliphatic polyester whose low immunogenicity provides an enormous opportunity to use it as a biomaterial in a variety of applications (particularly biomedical and as packaging materials). In fact, PCL is biodegradable, biocompatible, ecofriendly, easily processed, reasonably affordable and barrier-resistant (Azimi et al., 2014; Stepanova et al., 2019). By contrast, it has a low melting point and poor mechanical strength that can be improved by combination with other polymers (Rudnik, 2013; Terzopoulou et al., 2018). Wang et al. (2013) successfully synthesized chitosan-grafted-polycaprolactone by ROP in the ionic liquid [EMIM]Ac, using stannous octoate (Sn(Oct)2) as catalyst. In this work, PCL was for the first time grafted onto unmodified chitosan by using [EMIM]Ac for the first time (Wang et al., 2013). Numerous metal nanoparticles exist, and they have a wide range of possible uses. ZnO nanoparticles (ZnONPs) have aroused especial interest by virtue of their properties, which include excellent biological compatibility, intrinsic nontoxicity, low cost, UV shielding efficiency and antibacterial activity (Darshita and Sood, 2021). Roy and Rhim (2020) used ZnONPs as a catalyst for ROP of cyclic monomers in the absence of a conventional catalyst. Liao et al. (2006) synthesized PCL by caprolactone ROP in the presence of the ionic liquid (IL) (Roy and Rhim, 2020). Liao et al. (2006) synthesized PCL by ε-caprolactone ROP in the presence of the ionic liquid 1-butyl-3-methylimidazolium tetrafluoroborate, using zinc oxide as a catalyst. They found ZnO to catalyze CL ROP in the ionic liquid smoothly under microwave irradiation in the absence of an additional catalyst (Liao et al., 2006). Although ZnONPs have a variety of interesting applications, one key disadvantage is that they have a propensity to aggregate and agglomerate, which lowers the effectiveness of the resulting nanomaterials. Using an ionic liquid as the dispersion medium can solve this issue. Therefore, ILs operate as a "electrostatic shield" for metal nanoparticles, making them stable without the use of additional stabilizers, surfactants, or covering ligands (Aditya et al., 2018).

This paper reports a facile method for preparing cellulose-grafted-PCL nanocomposite films by partial dissolution and ring opening polymerization of ε-caprolactone monomers from a cellulose substrate. An ionic liquid was used as a smart nanowelding agent to assemble nanosized cellulose structures. Grafting of PLC from the cellulose substrate was used to reinforce the resulting transparent nanocomposite, and improve its mechanical and barrier properties as a result. ZnO nanoparticles and IL not only acted as catalysts for in situ ROP of ε-caprolactone monomers but also provided a nanocomposite with useful advantages including improved mechanical, barrier and optical properties, as well as improved antioxidant activity and UV-shielding efficacy (Fig. 1).

2. Materials and methods

2.1. Materials and film preparation

The bleached cotton linter pulp used as cellulose source was supplied by Celsur (Fonelas, Granada, Spain). The ionic liquid ([EMIM]Ac, 98%), a ZnO dispersion with particle size (40▓nm average particle size, 20▓wt% in H_2O), and ε-caprolactone (CL, 97%) were supplied by Sigma-Aldrich (Darmstadt, Germany). Distilled water was used as coagulant to remove residual IL. The procedure used to prepare transparent cellulose-grafted-PCL nanocomposite films, based on the results of various experimental tests, is briefly described here. The original paper was made from cotton linter pulp containing more than 90% α-cellulose as determined in accordance with TAPPI T203 and obtained by using a Rapid-Köthen former according to ISO 5269–2. First, 3▓mL of ionic liquid was mixed with variable amounts of caprolactone (10, 30, 50 or 70▓wt% base paper) and ZnONP dispersion (1, 3 or 5▓wt% base paper). The mixture was then stirred at 700▓rpm at 80°C for 30 min to induce ROP of caprolactone monomers for improved grafting efficiency. Then, a piece of dried paper (25▓mg aerial weight; 40 g/m^2 grammage; 64▓cm^2; 122 ± 4.08▓μm thickness) was placed in a glass Petri dish and the solution applied to its surface. The process was allowed to continue in an oven at 80°C for 24▓h. Afterwards, the gel film was rinsed many times in deionized water to remove any residual IL present in the regenerated sample. The nanocomposite film was allowed to dry between filter paper and a glass plate at 25°C at 50% relative humidity (RH) for at least 3 days. The resulting nanocomposite films were 48–61▓μm thick (see Table 1). The all-cellulose composite (ACC) film used as control sample was 48 ± 2.05▓μm thick and obtained by following the above-described procedure in the absence of ZnONPs and grafting PCL polymer chains.

2.2. Characterization of nanocomposite films

2.2.1. Degree of polymerization (DP) of cellulose

The limiting viscosity number in cupriethylenediamine (CED) solution was used for determining the viscosity index of cellulose in the cotton linter pulp, ACC and cellulose-grafted-PCL nanocomposite films according to ISO 5351 standard, using a capillary viscometer. The Mark-Houwink-Sakurada equation was used to calculate average DP.

2.2.2. Calculation of grafting parameters

Grafting parameters such as % grafting, % grafting efficiency and % homopolymer were calculated gravimetrically using the following equations (1)-(3), respectively (Villocillo and Angcajas, 2019):

$$Percent\ grafting\ (\%G) = \frac{(W_1 - W_o)}{W_o} \times 100 \quad (1)$$

$$Percent\ grafting\ efficiency\ (\%GE) = \frac{(W_1 - W_o)}{W_2} \times 100 \quad (2)$$

$$Percent\ homopolymer\ (\%H) = 100 - \%GE \quad (3)$$

Where W_o is the dry weight of the fiber treated with ionic liquid, W_1 and W_2 are the dry weights of cellulose-grafted-PCL nanocomposite film and ε-caprolactone monomer used in the reaction, respectively.

2.2.3. Structural properties

An X-ray diffractometer (PANalytical X'Pert PRO MPD Alpha1 powder diffractometer in a Bragg-Brentano $\theta/2\theta$ geometry of 240▓millimetres of radius) was used to record the nanocomposite films' X-ray diffraction patterns. The samples were analyzed at 1.5406▓Å radiation wavelength and 45▓kV-40▓mA with a 2° to 60° (2θ) scanning range. The crystallinity index (CI) was computed using the following equation (4) (Segal et al., 1959):

$$CrI\ (\%) = \frac{(I_200 - I_am)}{I_200} \times 100 \quad (4)$$

Where $I_2$00 is the intensity of the peak assigned to the (200) reflection of cellulose Iβ, which is typically in the range $2\theta = 21–23°$. I_am is the

minimum in the intensity occurs at about $2\theta = 18^{\circ}$ for noncrystalline cellulose. Scherrer's Eq. (5) was used for estimating the crystallite size:

$$D = \frac{K/\lambda}{\beta/cos\theta} \quad (5)$$

Where K is the constant of 0.9, λ is the wavelength of the incident X-ray (0.154056▓nm), β is the FWHM (Full width at half maximum) of the diffraction peak in radians, and θ is the diffraction angle corresponding to the planes (Lu et al., 2017).

An ATR-FTIR spectrophotometer was used to obtain fourier transform infrared spectra (Spectrum 100, Perkin Elmer, USA). Spectra were collected over a range of 4000–600▓cm^{-1}, with 64 scans overlapped and 1▓cm^{-1} resolution. The spectra's results were normalized.

A tridimensional (3D) roughness stylus profilometer was used to assess the samples' roughness (WYKO NT 1100 series Optical Profiling System, Veeco, Plainview, NY, USA).

FE-SEM (model JSM-7100 F, JEOL, USA) was used to examine the surface and cross-section of the produced nanocomposite films at a 10▓kV accelerating voltage. The samples were covered with a thin conductive coating of graphite prior to characterisation.

2.2.4. Barrier properties

The Bendtsen permeability tester (Chevron Co., USA) was used to test air permeance with 10 replicates in line with the ISO 5636–3:2013 standard.

MOCON OX-TRAN® Model 1/50 was used to calculate the oxygen transmission rate (OTR). The objective of test is to determine the amount of atmospheric oxygen concentration of 100% penetrates through the film's surface (50▓cm^2) in 24 h. The OTR tests were conducted at two temperatures and relative humidity levels: 23°C, 0% RH and 38°C, 90% RH, according to the ASTM D 3985 and F 1927 standards.

The nanocomposite films' water vapor permeability (WVP) was tested gravimetrically using the ASTM E96 standard method with minor modifications. The samples were initially preconditioned at 25°C and 50% RH for 24▓h in a constant temperature humidity chamber (model FX 1077, Jeio Tech Co. Ltd., Ansan, Korea) with an air movement of 198 m/min. The films were then placed on glass cups containing 3 g of calcium chloride (CaCl2) salt and sealed with a hot glue stick and parafilm to prevent water vapor penetration. After weighing the entire set, it was placed at 25 ± 2°C and 98 ± 2%RH by measuring the weight at intervals of 1 and 24▓h for 80▓h. The slope produced from a chart of weight gain vs. time using a simple linear regression method was used to compute water vapor transmission rate (WVTR) in ($g \cdot m^{-2} \cdot day^{-1}$). WVTR was calculated by dividing the slope of each line by the surface area of the sample exposed to water vapor, as shown in the following Eq. (6):

$$WVTR = \frac{(G/t)}{A} = \frac{slope}{test\ area} \quad (6)$$

Finally, the sample's WVP was calculated using the following Eq. (7) (Babaee et al., 2022):

$$WVP = \frac{WVTR}{P(R_1 - R_2)} \times X \quad (7)$$

Where X represents the film thickness (m), P indicates the water saturation vapour pressure at 25°C (Pa), R_1 shows the relative humidity in the chamber (98%RH), and R_2 refers the relative humidity in the cups (0% RH).

The water solubility (WS) of the sample was determined using a modified version of the approach used by Mohammadi et al. (2018b). The films were cut into squares of 2×2▓cm and dried in an oven at 105°C for 24▓hours to get the initial dry mass (W_1). After that, each film was placed in a bottle with 30 mL distilled water and agitated for 24▓hours at 25 ± 2°C. After that, each film was dried in the same manner in the oven and weighed (W_2). The film's water solubility was calculated using the following Eq. (8):

$$Water\ solubility\ (\%) = \frac{(W_1 - W_2)}{W_1} \times 100 \quad (8)$$

Where W_1 is the initial weight of dried film and W_2 is the final weight of dried film.

The water contact angle (WCA) was used to determine the hydrophobicity of the films. A WCA analyser (OCA15EC, Dataphysics Co., USA) was used to measure the contact angle of the nanocomposite films at a 25 frame/s image capture rate. A drop of distilled water (about 5▓μL) was poured on the surface of sample using a micro-syringe, and film stripes with a dimension of 1▓cm × 5▓cm were formed. Within 0–30▓seconds, the contact angle was established, and digital photographs were captured after 0 s. For each formulation, at least five samples were taken.

2.2.5. The thickness and optical properties

The thickness of nanocomposite films was measured through a micrometer (Frank-PTI digital 16502, Germany), according to ISO 534:2011. At least five random locations of each film sample was measured, and the mean value of these estimations was calculated as the film thickness.

A colorimeter (Technidyne, UK) was used to determine L^* (lightness), a^* (redness-greenness) and b^* (yellowness-blueness) as color parameters (Technidyne, UK). A white plate was used as a color reference (L = 92.92), and color parameters were determined at three random locations on the film's surface. The total color difference ($\triangle E$) between each color value of the standard color plate and film sample was obtained according to this following Eq. (9):

$$\triangle E = \sqrt{(L* - L)^2 + (a* - a)^2 + (b* - b)^2} \quad (9)$$

A UV–visible spectrophotometer (Evolution 600, Thermo Scientific) was used to assess the film's UV-barrier and transparency in the ultraviolet and visible ranges (200–800▓nm) as stated by Mohammadi et al. (2018b). The samples were first divided into rectangular strips (1▓cm x 3▓cm) before being inserted directly into the spectrophotometer's test cell. To assess the transparency and UV barrier properties of the samples, the transmittance at 600▓nm ($T600$) and 280▓nm ($T280$) were utilized. The transparency value was obtained according to this following Eq. (10):

$$Transparency\ (\%) = -log\frac{T600}{x} \quad (10)$$

$T600$ is the 600▓nm transmittance, x denotes the film thickness (mm). The higher transparency value presents, the lower nanocomposite films' transparency.

2.2.6. Mechanical properties

Mechanical parameters of various formulations were measured using a universal testing machine (JJ Lloyd instrument, model T5K) with a 500▓N load cell and a 50▓mm/min head speed. Film samples were cut into rectangular shapes with a length of 40▓mm and a width of 10▓mm for testing purposes. The films were conditioned for at least one week at 25°C and 50% relative humidity before mechanical testing. Tensile strength, elongation at break, tensile energy absorption, and Young's modulus were calculated directly from the stress-strain curves of five replicates for each film formulation.

2.2.7. Antioxidant activity

The antioxidant activity of the nanocomposite films was measured using 2, 2′-azinobis-(3-ethylbenzothiazoline-6-sulfonic acid) ($ABTS^+$) radical scavenging activity method according to Serpen et al. (2007) with modifications (Valls and Roncero, 2013; Cusola et al., 2015). In this method, the free radical scavenging activity was assessed by a

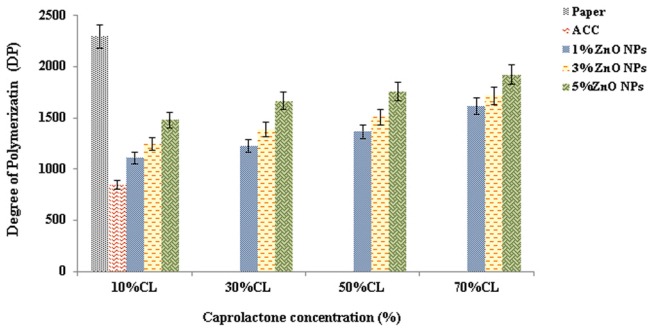

Fig. 2. Average degree of polymerization of cellulose in pulp, ACC and cellulose-grafted-PCL nanocomposite films with different contents in ZnONPs and CL.

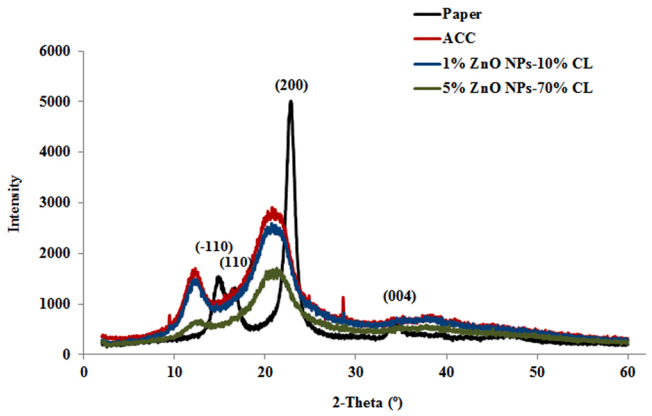

Fig. 3. XRD patterns for paper, ACC and cellulose-grafted-PCL nanocomposite films.

Table 2
Crystallinity index and crystallite size of cellulose in different samples.

Sample	Crystallinity index (%)	Crystallite size (nm)
Paper	89.36	6.75
ACC	46.58	1.5
Composite (1%ZnONPs,10% CL)	42.47	1.33
Composite (5%ZnONPs,70% CL)	41.62	1.26

spectroscopic method based on the disappearance of the absorption band at 752 nm of the free radical $ABTS^{+}$. To summarize, the $ABTS^{+}$ solution was created by oxidation of potassium persulfate. The solution was diluted to obtain an absorbance of 0.70 ± 0.1 at 752 nm. For comparison, 10 mg of nanocomposite film was vortexed for 2 minutes in 1.5 mL of $ABTS^{+}$ solution. The sample was then centrifuged for 4 minutes at 6000 rpm. Finally, the sample was maintained at room temperature for 30 minutes in the dark and the absorbance was determined at 752 nm. In the same process, the absorbance of a film-free control sample was evaluated at 752 nm. For each sample, the antioxidant activity was assessed at least three times. The antioxidant activity of the nanocomposite film was calculated according to the following Eq. (11):

$$Antioxidant\ activity\ (\%) = \frac{(A_o - A_1)}{A_o} \times 100 \quad (11)$$

A_1 is the absorbance of the nanocomposite film sample, while A_o is the absorbance of the control sample (without sample).

3. Results and discussion

3.1. Degree of polymerization (DP) of cellulose

Fig. 2 shows the average DP of the cellulose-grafted-PCL nanocomposite films, ACC and cotton linter pulp. DP for the initial pulp (2297) was reduced to 847 by partial dissolution (ACC), the latter value being is lower than that for the cellulose used as starting material. This result is fairly consistent with Duchemin et al. (2009). Adding CL monomers and ZnONPs to the cellulose matrix raised DP (from 1110 with 1% ZnONPs and 10% CL to 1923 with 5% ZnONPs and 70% CL). This result can be ascribed to DP being increased by a high content in noncellulose materials.

3.2. Grafting parameters

As might be expected, there were considerable influences on the grafting parameters depending on the amount of ε-caprolactone monomer in the reaction media. According to Table 1, the percentage of grafting increased significantly as CL increased; the highest percentage of grafting (38.2%) was attained at 70% CL in the nanocomposite film containing 1% ZnONPs. When the concentration of ZnONPs was raised further (by 5%), the percentage of grafting rose to 47.8%. According to Liao et al. (2006) and Kaur et al. (2014), an increase in grafting percentage was observed because the grafting process was stimulated by the higher ZnONPs concentration. The efficiency of grafting increased as monomer concentration rose. Low grafting efficiency indicates that fewer monomers were employed during grafting, and the majority of them were lost to side reactions and homopolymer synthesis. Additionally, in terms of grafting effectiveness, the percentage of homopolymer displayed an opposite trend. This effect can be explained by the monomer building up near to the cellulose backbone (Villocillo and Angcajas, 2019; Sand et al., 2010).

3.3. Structural properties

XRD spectra were used to examine the crystallographic properties of the cotton linter paper, ACC film, and cellulose-grafted-PCL nanocomposite films with the highest and lowest contents in ZnONPs and CL monomers (Fig. 3).

Table 2 shows their crystalline index and crystallite size. The peaks at the $2\theta = 14.8^{\circ}$, 16.6°, 22.8°, and 34.6° in the XRD spectrum for cotton linter are typically ascribed to cellulose I and assigned to diffraction planes (-110), (110), (200), and (004), respectively (Wu et al., 2016). The diffraction pattern for the ACC film after partial breakdown and coagulation from solution exhibited peaks at the $2\theta = 12.2^{\circ}$ (-110) and 20.7° (110) corresponding to the crystalline form of cellulose II. The crystallinity index of cotton paper was significantly higher than that of the ACC film. The loss of crystallinity and decrease in crystallite size from 6.75 to 1.50 nm can be ascribed to partial dissolution in the ionic liquid and the resulting destruction of crystalline structures and increase in the number of disordered chains in the cellulose matrix. This result is in line those of Lu et al. (2017) and Yousefi et al. (2015). Unlike those of the ACC film, the XRD patterns for the nanocomposite films remained unchanged upon grafting to PCL. Therefore, the regenerated cellulose matrix retained the original crystalline structure and crystallite size upon grafting to PCL chains (Wu et al., 2016). The crystallinity index of the cellulose-grafted-PCL nanocomposite containing 1% ZnONPs and 10% CL was 42.47% lower than that of ACC film. Graft copolymerization with the highest proportion of CL and ZnONPs slightly decreased the index (to 41.62%).

Fig. 4 shows the FTIR spectra for the original paper, ACC and nanocomposite films with in various monomeric CL to ZnONP ratios. As can be seen, the FTIR spectrum for native cellulose was quite similar to that for ACC and the nanocomposite films, which suggests that [EMIM]Ac and ZnONPs had no effect on the chemical structure of cellulose

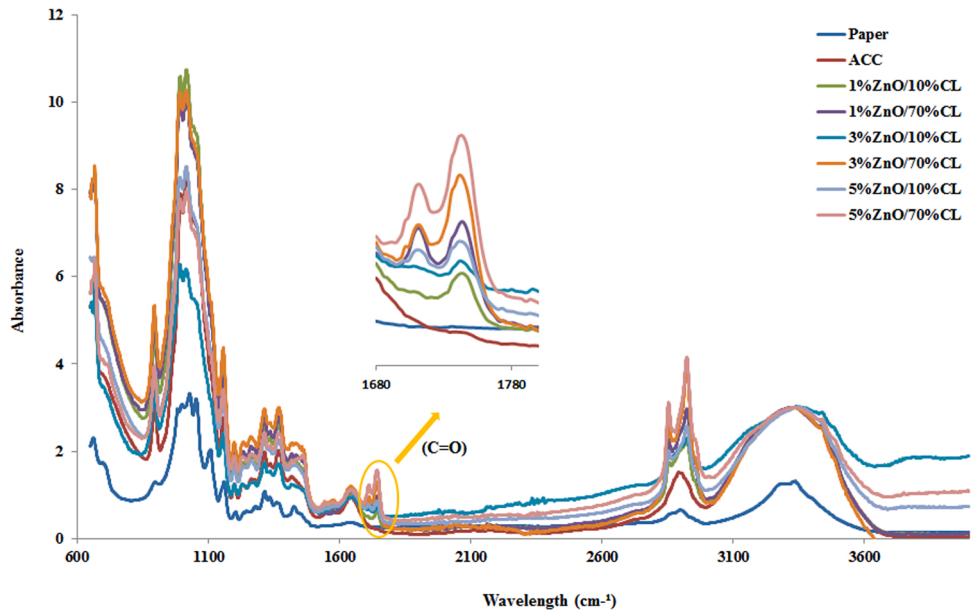

Fig. 4. FTIR spectra over the wavenumber range 4000–650 cm^{-1} for paper, ACC, and cellulose-grafted-PCL nanocomposite films with different contents in ZnONPs and CL.

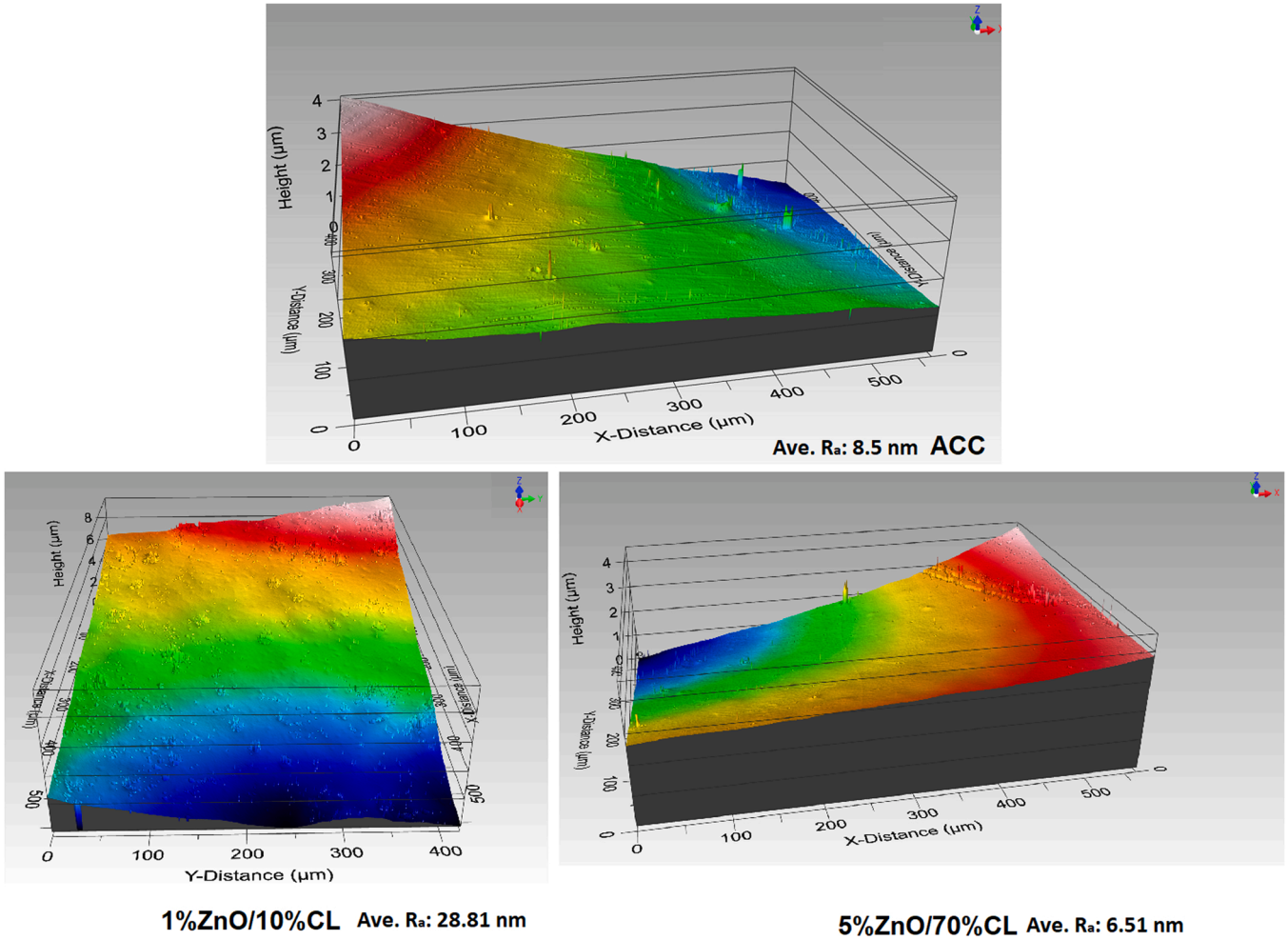

Fig. 5. Surface roughness of ACC and cellulose-grafted-PCL nanocomposite films with low and high ZnONPs and CL contents as determined from 3D profiles.

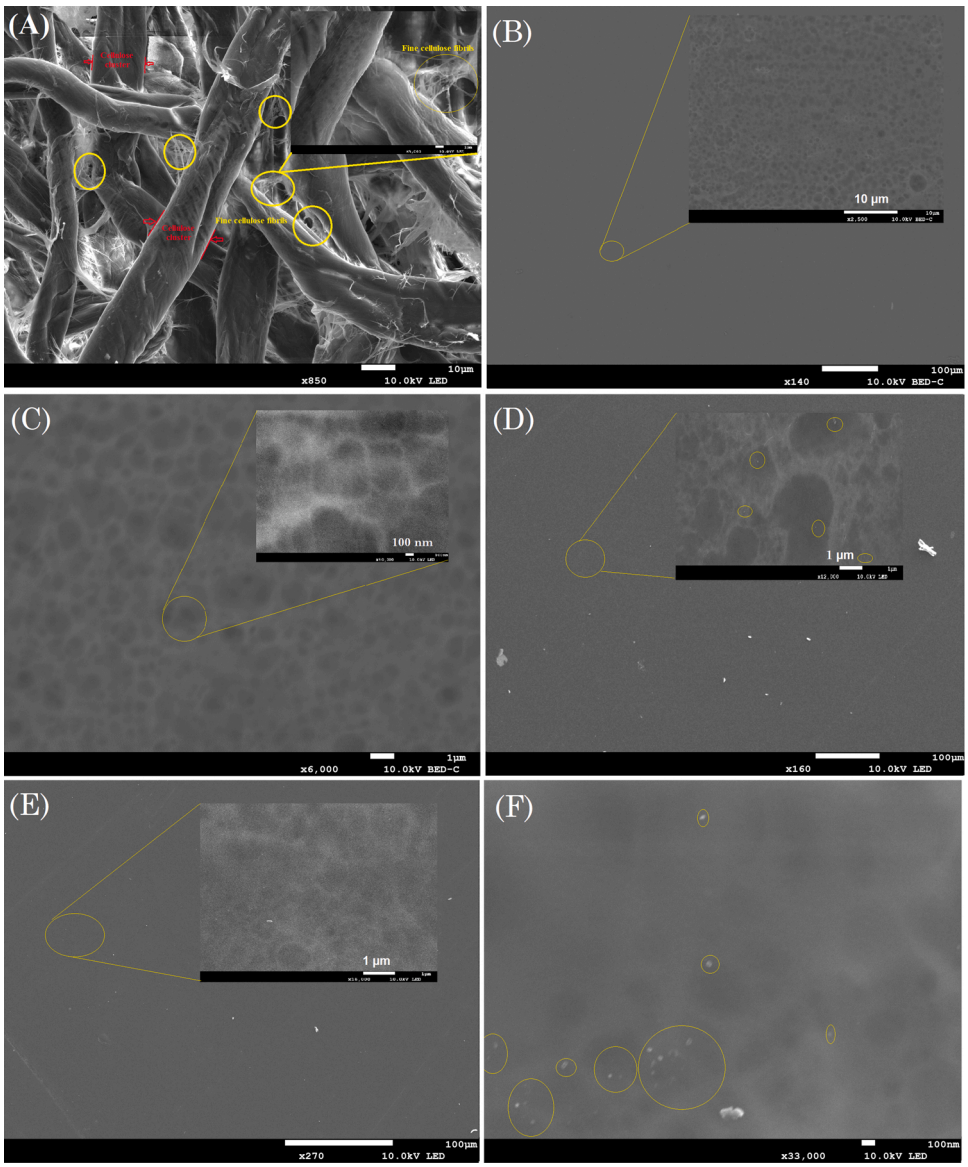

Fig. 6. SEM images at different magnifications illustrating the surface morphology of (A) paper; (B,C) ACC; (D) a nanocomposite film containing 1% ZnONPs and 10% CL and (E,F) a nanocomposite film obtained with 5% ZnONPs and 70% CL.

during the dissolution and regeneration process (Dissanayake et al., 2018; Yu et al., 2018).

There were three distinct differences between the spectra for the cellulose-grafted-PCL nanocomposite films and that for the cotton paper. According to Wang et al. (2017) and Zuppolini et al. (2020), the peaks at 2923 and 2855 cm^{-1} can be assigned to asymmetric and symmetric C-H stretching, respectively, of methyl groups in grafted PCL chains (Wang et al., 2017; Zuppolini et al., 2020). Their strength increased with increasing content in CL monomers and ZnONPs in the regenerated cellulose matrix. The characteristicpeak at 1742 cm^{-1}, assigned to C═O stretching of ester groups in PCL molecules, was absent from the spectra for the cotton paper and ACC film. Ring opening copolymerization of ε-caprolactone with cellulose was confirmed by the increased intensity of this peak (Dissanayake et al., 2018; Yu et al., 2018). In fact, based on normalized spectra, the peak grew in strength as the contents in CL monomers and ZnONPs of the copolymer were increased. Therefore, the amount of PCL grafted from the surface can be adjusted through the proportions of monomeric CL and ZnONPs. All samples exhibited broad bands at about 3000–3650 cm^{-1} that were assigned to stretching vibrations in -OH groups (Fu et al., 2015; Xu et al., 2019). Overall, our results suggest that cellulose I crystallized into cellulose II in the nanocomposite films. This was confirmed by the weakening in the typical bands for cellulose I at 1430 and 1110 cm^{-1} in the spectra for the ACC and nanocomposite films, which are strong in the spectrum for cotton cellulose (Pang et al., 2015; Dissanayake et al., 2018). The bands at 1565 and 1415 cm^{-1} corresponded to stretching of C-N and C = N bonds in [EMIM]Ac, which were absent from ACC and the cellulose-grafted-PCL nanocomposites. Therefore, the washing treatment successfully removed most [EMIM]Ac from fibers (Reyes et al., 2018; Chen et al., 2020b).

The nanocomposites with the highest and lowest contents in PCL and ZnONPs were used to assess roughness. The results are shown in Fig. 5. The ACC film had a relatively smooth and compact surface, whereas the composite containing 1% ZnONPs and 10% CL had a rough surface. These results are in line with those of previous work were ZnONPs increased the overall roughness of the polymer matrix (Moura et al., 2019; Vannozzi et al., 2020). Dispersing a 5% ZnONP concentration and a 70% CL concentration in the cellulose matrix decreased the average surface roughness significantly (6.51 nm), probably by diminishing pore size relative to the regenerated cellulose (8.5 nm) and the

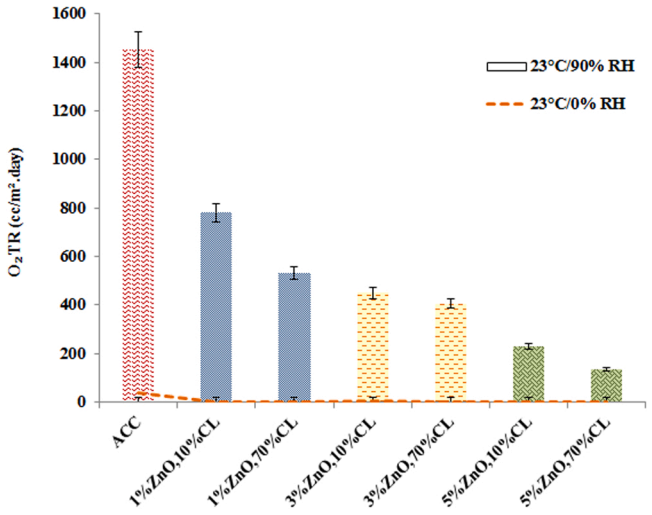

Fig. 7. OTR for ACC and cellulose-grafted-PCL nanocomposite films with different contents in ZnONPs and CL.

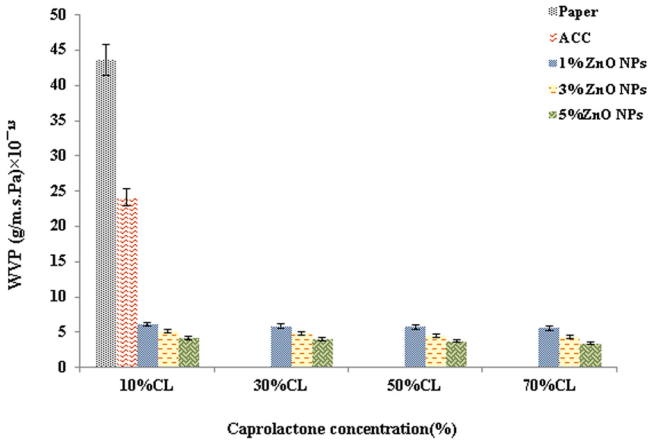

Fig. 8. Water vapor permeability of paper, ACC and cellulose-grafted-PCL nanocomposite films with different contents in ZnONPs and CL.

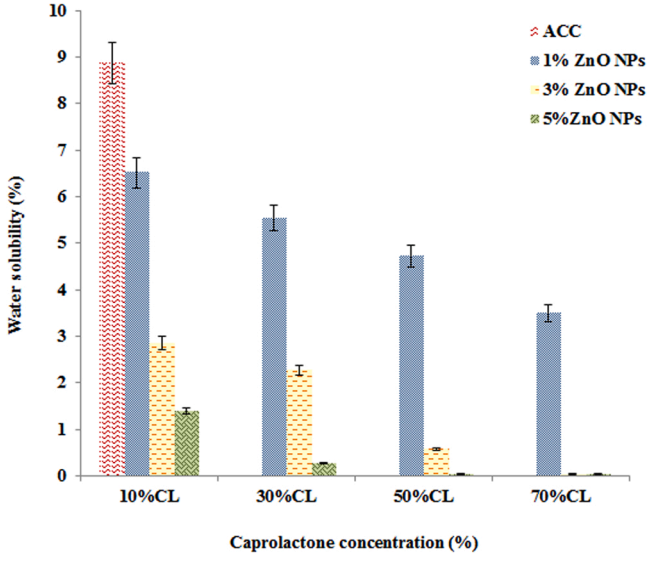

Fig. 9. Water solubility of paper, ACC and cellulose-grafted-PCL nanocomposite films with different contents in ZnONPs and CL.

polyethylene terephthalate plastic substrate (7.0 nm). Increasing the CL monomer content led to a more uniform, smoother surface texture, probably through effective interaction between ZnONPs and the polymer matrix influencing the overall roughness of the matrix (Mousa et al., 2018). Based on these results, the roughness of the nanocomposite films decreased and their surface smoothness increased with increasing concentration of CL monomers.

Micro- and nanostructures in the sample surfaces were examined by SEM to study the properties of the nanocomposite films. The results are shown in Fig. 6 at variable magnifications.

Fig. 6a shows an extremely open and porous network of unevenly crossing fibers in the original paper. When the IL efficiently promoted disintegration of cellulose fibers, it resulted in a smoother, more uniform surface. Also, with a dense liquid, fibers were entirely disassembled and a new structure was formed. Fig. 6b and c show the surface of the ACC film, which is consistent with the profilometric 3D roughness data. The surface contained some micro- and nanoholes that facilitated embedding of ZnONPs inside. PCL and ZnONP grafting, and dispersion in the regenerated cellulose matrix, was assessed by examining composites with the highest and lowest PCL and ZnONPs contents. As can be seen from Fig. 6d, nanoparticles were well disseminated and PCL was successfully grafted onto the cellulose matrix. Despite the hydrophobicity of PCL and hydrophilicity of cellulose, PCL and cellulose fibers proved compatible, which is consistent with the results of (Lönnberg et al., 2011). With relatively low treatment concentrations (Fig. 6d), the nanocomposite had a smooth, uniform surface. Compared to the ACC film, embedding greater amounts of ZnONPs and grafting of PCL chains in the cellulose matrix led to most micro-holes and cavities being filled (Fig. 6e). Also, as can be seen from Fig. 6f, ZnO particles were completely lodged in the nanostructure (i.e., they were trapped in nanofibrils after the cellulose matrix was regenerated).

3.4. Barrier properties

Similarly to the polyethylene and polypropylene packaging polymers used as controls, the cellulose-grafted-PCL nanocomposites and the ACC film were completely impermeable to air (air permeability = 0 $\mu m. Pa^{-1} \cdot s^{-1}$). This was a result of their totally consolidated nanostructures, which were welded together by trapped ZnONPs and prevented entry of tiny air molecules (Yousefi et al., 2015).

Fig. 7 shows the oxygen transmission rate of the cellulose-grafted-PCL nanocomposite films. At 0% RH, the films exhibited excellent oxygen barrier behavior of a combination of ZnONPs and PCL in cellulose matrix. The oxygen transmission rate (OTR) at 90% RH in the nanocomposite films was significantly lower than in the ACC film. Also, OTR decreased with increasing proportion of ZnONPs and CL monomers in the regenerated cellulose matrix.

The uniform distribution of ZnONPs and PCL chains in the film matrix led to a rapid fall in OTR values at 0%RH. The barrier properties of the nanocomposite films suffered at 90% RH, however, as a result of cellulose swelling and potentially cracking as humidity rises (Wu et al., 2019; Ahmed et al., 2017). At 90% RH, increasing the content in CL monomers of films with 5% ZnONPs decreased OTR by 82% relative to the nanocomposite containing 1% ZnONPs and 10% CL. Unlike the ACC film, entangled PCL and ZnONPs successfully resisted swelling, thereby resulting in fewer cracks and lower OTR. The decreased OTR values of the nanocomposite films were possibly due to the formation of a tortuous lane for oxygen by well-dispersed ZnONPs and PCL in the cellulose matrix (Koppolu et al., 2019; Roy et al., 2021). Many applications, but particularly food packaging, require high oxygen barrier capabilities. However, no specific rating scales have been established for barrier grades. Based on the estimated OTR values in the ranges 10, 1000 and 10,000 $cc \cdot m^{-2} \cdot day^{-1}$ at 23°C at 50% RH, Abdellatief and Welt (2013) categorized films as “high oxygen barrier”, “medium oxygen barrier”, and “low oxygen barrier”. Polyethylene terephthalate (PET), which has an OTR value of roughly 110 $cc \cdot m^{-2} \cdot day^{-1}$, is

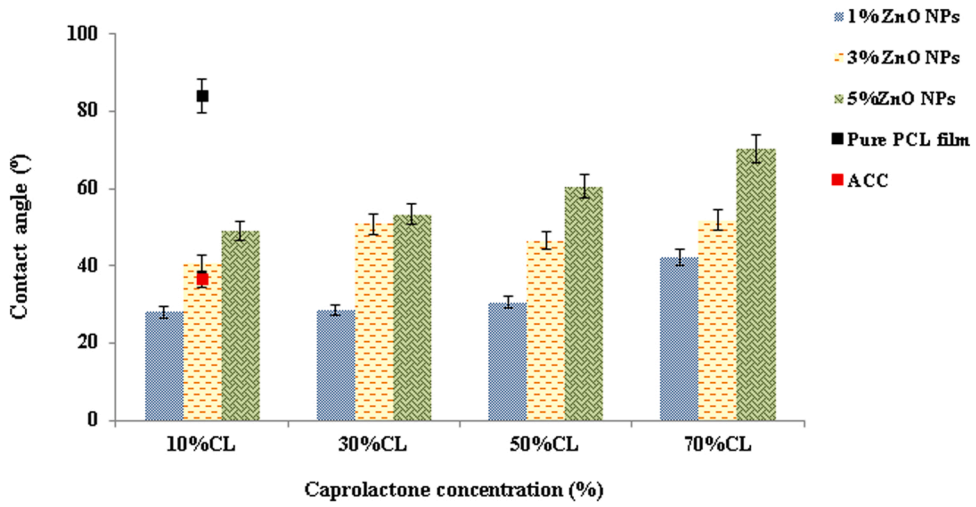

Fig. 10. Water contact angle of paper, ACC and cellulose-grafted-PCL nanocomposite films with different contents in ZnONPs and CL.

Table 3
Thickness and color of the cellulose-grafted-PCL films.

Sample	Thickness (μm)	L	a	b	$\triangle E$
ACC	48 ± 2.05	88.75 ± 0.05	− 1.32 ± 0.03	3.25 ± 0.05	4.24 ± 0.15
1% ZnO,10% CL	48 ± 2.05	89.83 ± 0.85	− 1.29 ± 0.03	3.13 ± 0.12	3.21 ± 0.86
1% ZnO,30% CL	51 ± 1.35	89.35 ± 1.02	− 1.31 ± 0.02	3.27 ± 0.07	3.70 ± 0.85
1% ZnO,50% CL	54 ± 1.75	89.45 ± 0.63	− 1.31 ± 0.03	3.37 ± 0.07	3.63 ± 0.62
1% ZnO,70% CL	58 ± 1.23	89.07 ± 0.25	− 1.27 ± 0.01	3.42 ± 0.06	3.96 ± 0.23
3% ZnO,10% CL	48 ± 1.20	89.58 ± 0.25	− 1.25 ± 0.07	3.08 ± 0.03	3.39 ± 0.14
3% ZnO,30% CL	52 ± 1.30	89.31 ± 0.7	− 1.30 ± 0.005	3.33 ± 0.05	3.74 ± 0.70
3% ZnO,50% CL	54 ± 0.50	89.33 ± 0.07	− 1.29 ± 0.04	3.51 ± 0.17	3.81 ± 0.10
3% ZnO,70% CL	60 ± 0.85	89.36 ± 0.59	− 1.33 ± 0.01	3.37 ± 0.18	3.73 ± 0.53
5% ZnO,10% CL	50 ± 1.25	89.19 ± 0.78	− 1.28 ± 0.01	3.39 ± 0.05	3.84 ± 0.77
5% ZnO,30% CL	53 ± 1.56	89.04 ± 0.31	− 1.22 ± 0.11	3.21 ± 0.47	3.95 ± 0.33
5% ZnO,50% CL	54 ± 1.30	89.13 ± 0.58	− 1.26 ± 0.005	3.39 ± 0.14	3.90 ± 0.53
5% ZnO,70% CL	61 ± 0.65	88.65 ± 0.34	− 1.3 ± 0.03	3.17 ± 0.08	4.32 ± 0.37

currently the most extensively used commercial food packaging material (Abdellatief and Welt, 2013). Based on their OTR values, our nanocomposite films can be used as packaging materials for food, pharmaceuticals (tablets), fresh meat and peanuts because, based on research by Gao et al. (2020), Wang et al. (2018), and Markus et al. (2012), the required OTR values for these uses are less than 100, 80 and 50 $m^{-2} \cdot day^{-1}$, respectively (Gao et al., 2020; Wang et al., 2018; Markus et al. 2012).

Water vapor permeability (WVP) is an essential property for packaging applications. Fig. 8 shows the WVP values for the samples as compared to the controls (ACC and paper). The value for ACC was roughly 68% lower than that for untreated paper, a result suggesting that welding improved the barrier properties of microfibers with an increased porosity (Reyes et al., 2018).

WVP for the cellulose-grafted PCL films fell in the range (3.4–6.1) $\times 10^{-13} g/m.\ s.\ Pa$. Introducing 1% ZnONPs and 10% CL into the cellulose matrix decreased WVP from 24.1 $\times 10^{-13} g/m.\ s.\ Pa$ for the ACC film to 3.4 $\times 10^{-13} g/m.\ s.\ Pa$. Clearly, ZnONPs and CL had a synergistic effect. However, there was no clear difference in WVP between the nanocomposite film containing 1% ZnONPs plus 10% CL and those with loaded with greater amounts of the two components, which were similar to one another in this respect. WVP was reduced by effect of the uniform dispersion and hydrophobicity of the materials in the cellulose matrix (Reis et al., 2021). Through interaction of the two processes, inorganic nanoparticles such as those of ZnO can improve the barrier properties of polymers. First, by replacing a permeable polymer, impermeable nanoparticles reduce the area that can be accessed for diffusion. Second, permeants must take a circuitous route around impermeable nanoparticles to pass through films, thereby travelling increased distances (Reis et al., 2021). Also, discreet ZnONPs in the film matrix obstruct motion of PCL polymer chains grafted on the surface of regenerated cellulose. Finally, ZnONPs restricting the mobility of PCL chains can have a favorable impact on WVP in nanocomposite films. Kanmani and Rhim (2014) and Mohammadi et al. (2018a), came up with a similar finding. Other polymers materials such as starch and chitosan are typically biodegradable and have ultrahigh WVP values [3.87 $\times 10^{-10}$ and (3.66–4.80) $\times 10^{-11} g/m.\ s.\ Pa$, respectively. Polyethylene terephthalate (PET), polyvinyl dichloride (PVDC), low-density polyethylene (LDPE), high-density polyethylene (HDPE) and cellophane are all commercially available conventional petroleum-based food packaging materials with ultrahigh barrier properties (WVP values in the region of 3.3 $\times 10^{-12}$, 2.31 $\times 10^{-13}$, 9.14 $\times 10^{-13}$, 2.22 $\times 10^{-13}$ and 8.4 $\times 10^{-11} g/m.\ s.\ Pa$, respectively) (Zhang et al., 2022). The nanocomposite film obtained with 1% ZnONPs and 10% CL here had a higher WVP than starch and chitosan. Therefore, cellulose-grafted-PCL nanocomposite film can be deemed ultrahigh WVP barrier materials suitable for commercial food packaging as they are not vulnerable to water vapor.

As can be seen from Fig. 9, increasing the amounts of ZnONPs and CL monomers in the cellulose-grafted PCL nanocomposite films reduced their water solubility relative to ACC. The films containing 3% or 5% ZnONPs were more resistant to dissolution by water than were those containing 1% ZnONPs. Raising the CL content to 70% significantly

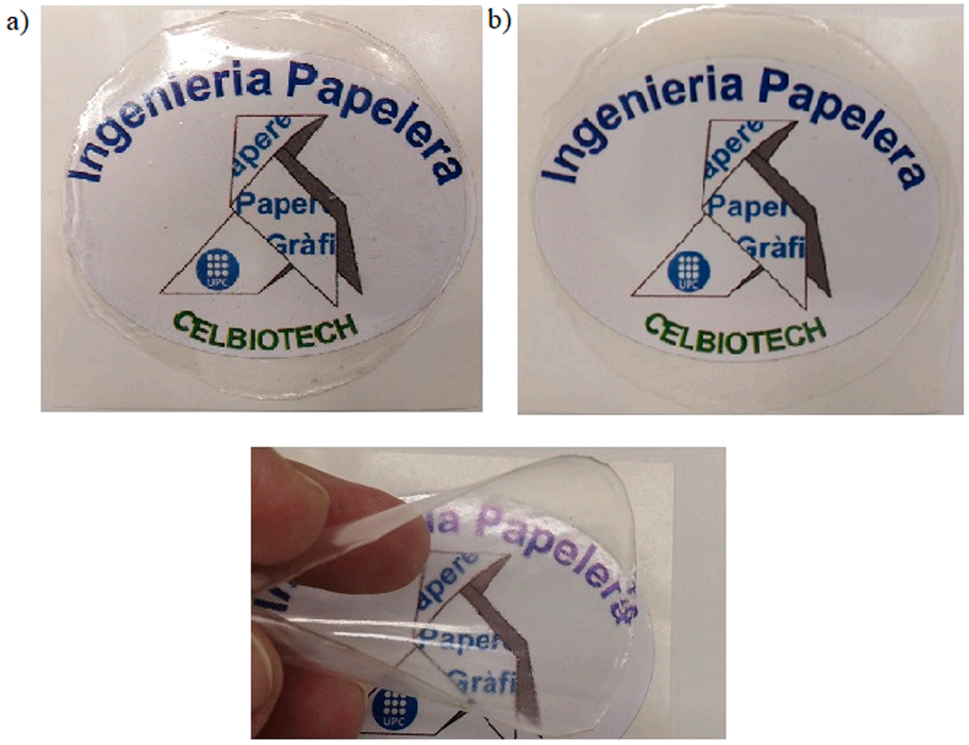

Fig. 11. Visual appearance, qualitative transparency and flexibility of cellulose-grafted PCL nanocomposite films containing (a) 1% ZnONPs and 10%CL; and (b) 5% ZnONPs and 70% CL.

decreased water solubility. Thus, the films containing 5% ZnONPs and 50 or 70% CL were completely insoluble in water. The water solubility of the films dropped owing to the reduced hydrophilicity resulting from the incorporation of ZnONPs and PCL chains, which decreased the accessibility of free OH groups (Roy et al., 2021; Jamróz et al., 2019).

The effect of ZnONPs and PCL on the surface hydrophobicity of cellulose-grafted-PCL nanocomposite films was assessed from water contact angle (WCA) measurements (Fig. 10). The presence of hydroxyl groups in the nanocomposite decreased WCA relative to PCL film. The samples containing 1% ZnONPs showed no substantial change in WCA. Increasing proportions of CL monomers and ZnONPs added to the matrix resulted in also increasing WCA values. Thus, WCA increased from 28.02˚ in the sample containing 1% ZnONPs and 10% CL to 50.84˚ in that containing 3% ZnONPs and 30% CL, and 60.51˚ in the nanocomposite with 5% ZnONPs and 50% CL. WCA for the film obtained with 5% ZnONPs and 70% CL was even higher: 70.35˚. Incorporating increased amounts of ZnONPs and PCL into the cellulose matrix increased WCA by reducing free hydrophilic groups in the cellulose structure and increasing fiber hydrophobicity as a result. A similar increase in WCA by effect of incorporating ZnONPs into cellulose-based films was previously observed by Noshirvani et al. (2017) and Azari et al. (2021).

3.5. Thickness and optical properties

Table 3 shows the thickness of the cellulose-grafted-PCL films. The thickness of the ACC film (48 ± 2.05 μm) was smaller than that of the original (122 ± 4.08 μm) by effect of the welding agent facilitating the formation of a more compact surface than that of macrofibers in the original paper. Film thickness increased from 0.048 mm to 0.061 mm as increasing amounts of LA and ZnONPs were added to the cellulose matrix.

Fig. 11 illustrates the flexibility and plasticity of cellulose-grafted-PCL nanocomposite films. All were adequately flexible and transparent. The color of packaging films has a considerable impact on the visual appearance of the food products they contain and their acceptance by consumers. Table 3 shows the color-related parameters L^* (lightness), a^* (green-red), b^* (blue-yellow) and $\triangle E$ for the different formulations. As can be seen, there were no significant differences in the previous parameters between films containing 1–5% ZnONPs except for that obtained with 5% ZnONPs and 70% CL, which had a reduced lightness and an increased $\triangle E$ value as a result. Saedi et al. (2021) found L^* to decrease and $\triangle E$ to increase as more ZnONPs were added to cellulose-based films Saedi et al. (2021).

The cellulose-grafted-PCL nanocomposite films were tested for UV and visible light transmission at 280, 350, 400, and 660 nm, respectively (Table 4). One of the main factors influencing food deterioration and nutrient loss is UV irradiation, particularly in UVA (320–400 nm) and UVB (290–320 nm) regions (Xiao et al., 2022). As demonstrated, ACC film possessed a high level of UV transparency. When ZnONPs were introduced to nanocomposite films, the transmittance in the UV area kept declining without significantly affecting visible light transmittance a desirable feature for food packaging materials. The film containing 5% ZnONPs and 70% CL had the lowest UV light transmittance (46.19%) and visible light transmittance (78.30%) and hence the best UV–vis light barrier properties. Therefore, increasing the contents in CL and ZnONPs of the nanocomposite films allowed them to successfully block UV and visible light. Light transmittance was significantly reduced by effect of ZnO nanoparticles scattered in the cellulose-grafted PCL matrix inhibiting light passage (Shankar et al., 2018). The fact that light transmission in the cellulose-grafted-PCL composite films was lower in the UV region than it was in the visible range suggests that the films efficiently blocked UV light penetration without sacrificing transparency. Table 3 shows the transparency of the films as measured at 600 nm. The lower the transparency index was, the more transparent was the film. There were no significant differences in transparency index among films containing 1–5% ZnONPs. In summary, cellulose-grafted-PCL nanocomposite films with a ZnONP proportion of 5% proved efficient UV light barriers, which is an important feature for food packaging and bioproduct preservation.

Table 4
Light transmittance (%) at different wavelength (nm) and transparency value of cellulose-grafted-PCL films.

Sample	280	350	400	660	Transparency value
ACC	81.90 ± 0.76	83.42 ± 0.92	84.33 ± 0.66	85.42 ± 0.42	3.03 ± 0.03
1% ZnO,10% CL	69.92 ± 2.13	75.74 ± 0.33	77.33 ± 0.54	85.01 ± 1.19	3.11 ± 0.03
1% ZnO,30% CL	67.86 ± 1.05	72.05 ± 1.55	75.09 ± 1.61	85.63 ± 1.29	3.01 ± 0.08
1% ZnO,50% CL	64.69 ± 3.35	71.03 ± 1.2	74.45 ± 1.34	86.01 ± 1.98	3.19 ± 0.01
1% ZnO,70% CL	60.49 ± 2.37	68.76 ± 1.27	72.74 ± 1.18	85.15 ± 0.85	3.15 ± 0.01
3% ZnO,10% CL	61.60 ± 2.92	69.12 ± 0.21	72.48 ± 1.67	87.09 ± 1.41	3.20 ± 0.02
3% ZnO,30% CL	60.87 ± 2.49	67.48 ± 1.43	73.26 ± 1.37	85.25 ± 1.04	3.16 ± 0.03
3% ZnO,50% CL	60.17 ± 2.05	66.25 ± 1.16	71.45 ± 1.65	83.01 ± 1.57	3.15 ± 0.07
3% ZnO,70% CL	57.17 ± 2.05	65.30 ± 0.56	69.65 ± 1.40	84.75 ± 1.57	3.10 ± 0.07
5% ZnO,10% CL	56.42 ± 1.57	62.23 ± 1.30	67.67 ± 0.85	83.81 ± 1.38	3.04 ± 0.02
5% ZnO,30% CL	50.0 ± 2.27	60.36 ± 0.87	66.76 ± 1.56	84.46 ± 1.38	3.09 ± 0.05
5% ZnO,50% CL	47.51 ± 1.33	59.43 ± 0.54	65.36 ± 1.28	80.65 ± 0.97	3.04 ± 0.06
5% ZnO,70% CL	46.19 ± 1.67	59.19 ± 1.08	65.21 ± 1.15	78.30 ± 1.29	3.02 ± 0.13

3.6. Mechanical testing

Fig. 12 shows the tensile strength (TS), elongation at break (EB), tensile energy absorption (TEA) and Young's modulus (YM) of the base paper, ACC film and various cellulose-grafted-PCL nanocomposites. The tensile properties of the nanocomposites were affected by the incorporation of ZnONPs and PCL. Thus, TS for the base paper was only 0.6▓MPa but significantly increased (to around 80▓MPa) after dissolution in the ionic liquid. The increase can be ascribed to the IL acting as a nanowelding agent to connect smaller fibers in nanostructures and create a tighter network with more junction points as a result. The bulk and surface of the cellulose were probably plasticized by [EMIM]Ac during the nanowelding process, leading to increased ductility. This result is consistent with the conclusions of Ghaderi et al. (2014), Yousefi et al. (2011), and Niu et al. (2019).

As can be seen in Fig. 12a, tensile strength increased with increasing contents in ZnONPs and CL of the nanocomposites. Thus, TS for the ACC film was increased by 30% after upon addition of 1% ZnONPs and 10% CL; also, it increased from 104.5 to 117▓MPa with increase in ZnONPs from 1% to 5% at 70% CL. According to Beikzadeh et al. (2021), an increase in tensile strength can be ascribed to factors such as the rigidity of the nanofiller, its ease of dispersion and powerful interfacial connections between the film components and the matrix (Beikzadeh et al., 2021). Adding variable amounts of ZnO nanoparticles increased the elongation at break (EB) of the nanocomposite films that containing 3% ZnONPs and 10% CL excepted (Fig. 12b). EB for the film containing 5% ZnONPs and 70% CL, 57.9%, was considerably greater than that for the ACC film, which suggests that the nanocomposite was more flexible. This result can be ascribed to the stiff regenerated cellulose matrix and ZnONPs not restricting motion of PCL molecular chains. In previous work, the addition of 25% ZnONPs improved EB through good dispersion of the nanofiller in the PCL matrix (Gibril et al., 2019). TEA (the area under the stress-strain curve) is a measure of the ability of a material to absorb energy under tensile stress. TEA can be influential on film durability upon repetitive or dynamic stressing or straining. In fact, TEA is also a measure of sheet "toughness". As can be seen in Fig. 12c, increased proportions of ZnONPs and CL led to excellent TEA values for the nanocomposite films, which were thus more ductile (less brittle). Young's modulus (YM) relative to the ACC film peaked with the smallest amount of ZnONPs (Fig. 12d). YM was slightly increased by 1% ZnONPs but decreased by higher proportions of nanoparticles. This result is consistent with reports of Shankar et al. (2018). No significant differences in YM were observed with the addition of increasing amounts of CL to the regenerated cellulose matrix.

3.7. Antioxidant activity

The antioxidant activity of the cellulose-grafted PCL nanocomposite films is illustrated in Fig. 13. As can be seen, ABTS radical scavenging by the films remarkably improved upon addition of ZnO nanoparticles, which is consistent with previous results of Ananthalakshmi et al. (2019). The ACC film had negligible antioxidant activity because exposed electron-donating hydroxyl groups in the cellulose matrix reacted with free radicals over time (Priyadarshi et al., 2021). The pure PCL film also had poor antioxidant properties (2.5%). Antioxidant capacity was highest for the film obtained with 5% ZnONPs and 70% CL, and lowest for that containing 1% ZnONPs and 10% CL. The films with 1% ZnONPs and 10%, 30% or and 50% CL exhibited low antioxidant activity (viz., ABTS scavenging values of 6.01%, 7.91% and 8.23%, respectively). Scavenging rose to 13.75% with a CL content of 70%. Because PCL chains acted as a store and defense system for ZnONPs in the film matrix, increasing the CL loading considerably increased free radical scavenging activity in the films. This result can be ascribed to the films releasing more active compounds into the free radical solution and increasing ABTS radical inhibition as a result. An identical trend was observed in the films obtained with 3% or 5% ZnONPs and 70% CL, whose ABTS scavenging activity was 19.75% and 21.53%, respectively. These results suggest effective free radical inhibition with increased contents of not only ZnONPs, but also CL. Our results are consistent with those of Rezaeiet al. (2020), who investigated antioxidant activity in ZnONPs for use in active films (Rezaei et al., 2020).

4. Conclusions

We prepared cellulose-grafted-PCL nanocomposite film based on a regenerated cellulose matrix that was reinforced with ZnONPs and PCL. Gravimetric measurements and FTIR characterization indicate that the amount of grafting depends on the concentration of CL and ZnONPs present in the reaction medium. Also, SEM and XRD data testified to the good compatibility and intermolecular interaction between regenerated cellulose, ZnONPs and PCL. Adding ZnONPs and CL monomers to the cellulose matrix increased DP in the nanocomposites relative to the control films. Thus, adding 3 % or 5 % ZnONPs and 70 % CL to a regenerated cellulose matrix provided nanocomposite films of similar color, visible light transmission, transparency, water solubility, Young's modulus and tensile strength. On the other hand, ZnONPs increased the flexibility of the films by increasing their elongation at break and tensile energy absorption. The oxygen and water vapor barrier properties at 90 % RH of a nanocomposite film containing of 5 % ZnONPs and 70 % CL were 90 % and 85 %, higher, respectively than those of the ACC film. However, there was no clear difference in water vapor permeability between a film made with 1 % ZnONPs and 10 % CL, and others containing greater amounts of either or both. Based on physicomechanical

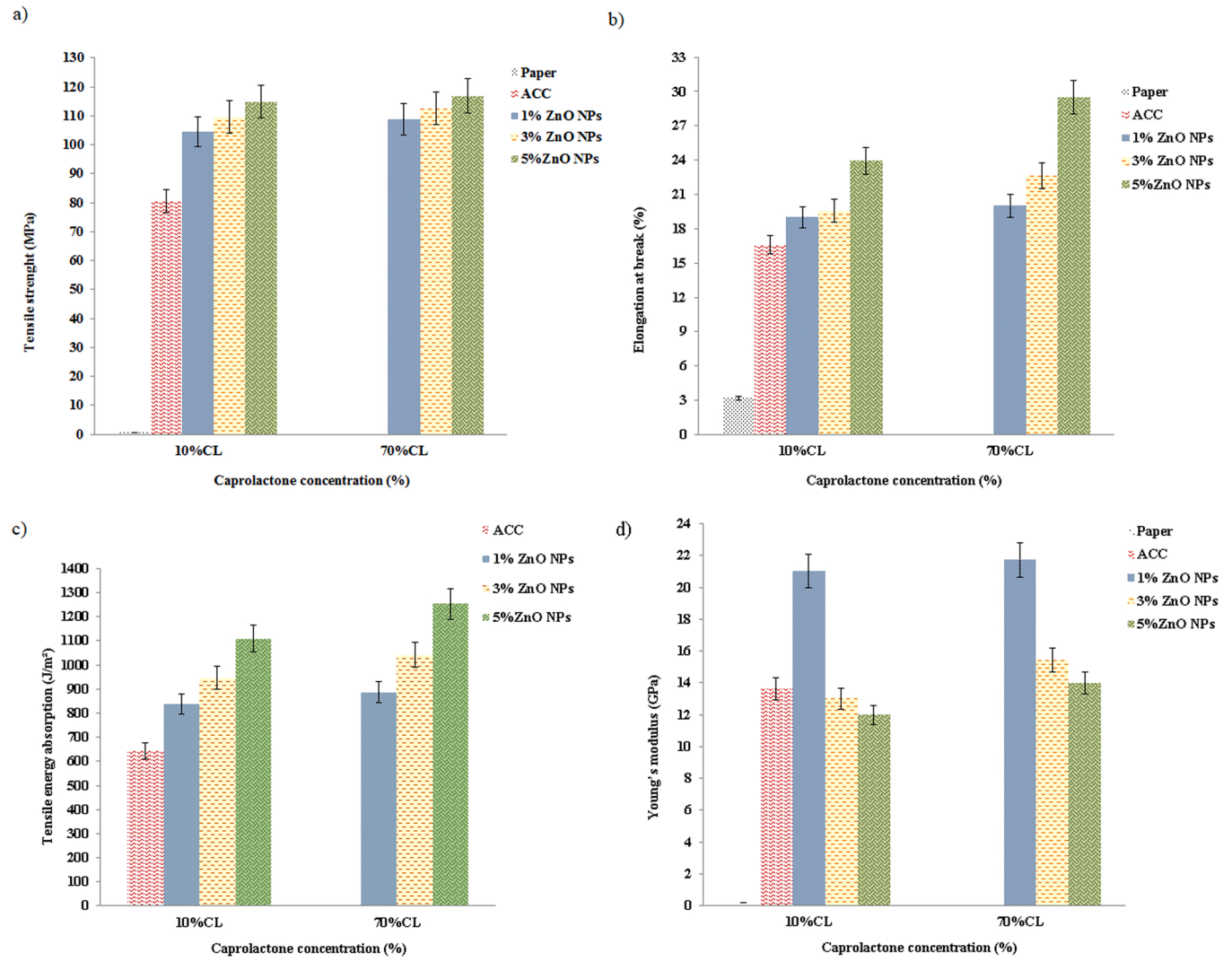

Fig. 12. Tensile strength (MPa), elongation at break (%), tensile energy absorption (J/m^2), and Young's modulus (GPa) of paper, ACC and cellulose-grafted-PCL nanocomposite films with different contents in ZnONPs and CL.

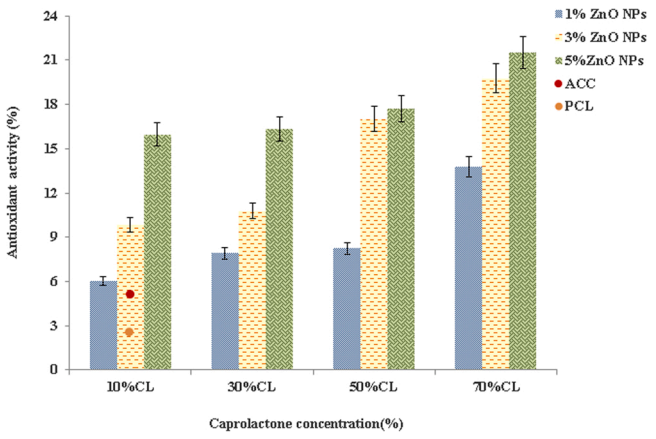

Fig. 13. Antioxidant activity of paper, ACC and cellulose-grafted-PCL nanocomposite films with different contents of ZnONPs and CL.

properties such as UV light transmittance, water vapor permeability, oxygen transmission rate, water solubility, tensile strength and Young's modulus, and on antioxidant properties, the optimum concentration of ZnONPs to be added to the cellulose matrix was 3 %. Based on our results, adding PCL polymers and ZnOPs to a regenerated cellulose matrix enhances its potential as a safe, active food packaging material.

Author's contribution

Conception and design of study: E. Amini, C. Valls and M.B. Ronceroacquisition of data: E. Aminianalysis and/or interpretation of data: E. AminiDrafting the manuscript: E. Aminirevising the manuscript critically for important intellectual content: C. Valls and M.B. RonceroApproval of the version of the manuscript to be published:E. Amini, C. Valls and M.B. Roncero

Declaration of Competing Interest

The authors declare that they have no known competing financial interests or personal relationships that could have appeared to influence the work reported in this paper.

Data Availability

No data was used for the research described in the article.

Acknowledgements

This publication is part of the PID2020-114070RB-I00 (CELLECO-PROD) project, funded by MCIN/AEI/10.13039/ 501100011033. The first author, E. Amini, gratefully acknowledges the Universitat Politècnica de Catalunya and Banco Santander for the financial support of her predoctoral grant FPI-UPC.

References

Abdellatief, Ayman, Welt, Bruce A., 2013. Comparison of new dynamic accumulation method for measuring oxygen transmission rate of packaging against the steady-state method described by astm d3985. Packag. Technol. Sci. 26 (5), 281–288.

Adak, Bapan, Mukhopadhyay, Samrat, 2016. Effect of the dissolution time on the structure and properties of lyocell-fabric-based all-cellulose composite laminates. J. Appl. Polym. Sci. 133 (19).

Aditya, Anusha, Chattopadhyay, Sabyasachi, Jha, Diksha, Gautam, Hemant K., Maiti, Souvik, Ganguli, Munia, 2018. Zinc oxide nanoparticles dispersed in ionic liquids show high antimicrobial efficacy to skin-specific bacteria. ACS Appl. Mater. Interfaces 10 (18), 15401–15411.

Ahmed, Jasim, Arfat, YasirAli, Al-Attar, Hassan, Auras, Rafael, Ejaz, Mohammad, 2017. Rheological, structural, ultraviolet protection and oxygen barrier properties of linear low-density polyethylene films reinforced with zinc oxide (zno) nanoparticles. Food Packag. Shelf Life 13, 20–26.

Amini, Elahe, Valls, Cristina, Roncero, M. Blanca, 2021. Ionic liquid-assisted bioconversion of lignocellulosic biomass for the development of value-added products. J. Clean. Prod. 326, 129275.

Ananthalakshmi, R., Rajarathinam, S.R., Mohamed Sadiq, A., 2019. Antioxidant activity of zno nanoparticles synthesized using Luffa acutangula peel extract. Res. J. Pharm. Technol. 12 (4), 1569–1572.

Azari, Shahin Sherafatkhah, Alizadeh, Ainaz, Roufegarinejad, Leila, Asefi, Narmela, Hamishehkar, Hamed, 2021. Preparation and characterization of gelatin/β-glucan nanocomposite film incorporated with zno nanoparticles as an active food packaging system. J. Polym. Environ. 29 (4), 1143–1152.

Azimi, Bahareh, Nourpanah, Parviz, Rabiee, Mohammad, Arbab, Shahram, 2014. Fiber: an overview. J. Eng. Fibers Fabr. 9 (3), 155892501400900309.

Babaee, Mehran, Garavand, Farhad, Rehman, Abdur, Jafarazadeh, Shima, Amini, Elahe, Cacciotti, Ilaria, 2022. Biodegradability, physical, mechanical and antimicrobial attributes of starch nanocomposites containing chitosan nanoparticles. Int. J. Biol. Macromol. 195, 49–58.

Beikzadeh, Samira, Hosseini, Seyede Marzieh, Mofid, Vahid, Ramezani, Soghra, Ghorbani, Marjan, Ehsani, Ali, Mortazavian, AmirMohammad, 2021. Electrospun ethyl cellulose/poly caprolactone/gelatin nanofibers: The investigation of mechanical, antioxidant, and antifungal properties for food packaging. Int. J. Biol. Macromol. 191, 457–464.

Carlmark, Anna, Larsson, Emma, Malmström, Eva, 2012. Grafting of cellulose by ring-opening polymerisation–a review. Eur. Polym. J. 48 (10), 1646–1659.

Chen, Ke, Xu, Weixin, Ding, Yun, Xue, Ping, Sheng, Pinghou, Qiao, Hui, He, Jimin, 2020a. Hemp-based all-cellulose composites through ionic liquid promoted controllable dissolution and structural control. Carbohydr. Polym. 235, 116027.

Chen, Pei, Xie, Fengwei, Tang, Fengzai, McNally, Tony, 2020b. Ionic liquid (1-ethyl-3-methylimidazolium acetate) plasticization of chitosan-based bionanocomposites. ACS Omega 5 (30), 19070–19081.

Cusola, Oriol, Valls, Cristina, Vidal, Teresa, Roncero, MBlanca, 2015. Conferring antioxidant capacity to cellulose based materials by using enzymatically-modified products. Cellulose 22 (4), 2375–2390.

M.N. Darshitaand Richa Sood.Review on synthesis and applications of zinc oxide nanoparticles.2021.

de Moura, Nayara Koba, Siqueira, Idália A.W.B., Paulo de Barros Machado, João, Kido, Hueliton Wilian, Avanzi, Ingrid Regina, Rennó, Ana Claudia Muniz, de Sousa Trichês, Eliandra, Passador, Fabio Roberto, 2019. Production and characterization of porous polymeric membranes of pla/pcl blends with the addition of hydroxyapatite. J. Compos. Sci. 3 (2), 45.

Dissanayake, Niwanthi, Thalangamaarachchige, Vidura D., Troxell, Shelby, Quitevis, Edward L., Abidi, Noureddine, 2018. Substituent effects on cellulose dissolution in imidazolium-based ionic liquids. Cellulose 25 (12), 6887–6900.

Duchemin, Benoît.J.C., Mathew, Aji P., Oksman, Kristiina, 2009. All-cellulose composites by partial dissolution in the ionic liquid 1-butyl-3-methylimidazolium chloride. Compos. Part A: Appl. Sci. Manuf. 40 (12), 2031–2037.

Fu, Feiya, Li, Lingyan, Liu, Lianjie, Cai, Jun, Zhang, Yaping, Zhou, Jinping, Zhang, Lina, 2015. Construction of cellulose based zno nanocomposite films with antibacterial properties through one-step coagulation. ACS Appl. Mater. Interfaces 7 (4), 2597–2606.

Gao, Qian, Lei, Min, Zhou, Kemeng, Liu, Xinliang, Wang, Shuangfei, Li, Huimin, 2020. Preparation of a microfibrillated cellulose/chitosan/polypyrrole film for active food packaging. Prog. Org. Coat. 149, 105907.

Ghaderi, Moein, Mousavi, Mohammad, Yousefi, Hossein, Labbafi, Mohsen, 2014. All-cellulose nanocomposite film made from bagasse cellulose nanofibers for food packaging application. Carbohydr. Polym. 104, 59–65.

Gibril, MagdiE., Ahmed, KumKum, Lekha, Prabashni, Sithole, Bruce, Khosla, Ajit, Furukawa, Hidemitsu, 2019. Effect of nanocrystalline cellulose and zinc oxide hybrid organic–inorganic nanofiller on the physical properties of polycaprolactone nanocomposite films. Microsyst. Technol. 1–10.

Grzabka-Zasadzińska, Aleksandra, Skrzypczak, Andrzej, Borysiak, Sławomir, 2019. The influence of the cation type of ionic liquid on the production of nanocrystalline cellulose and mechanical properties of chitosan-based biocomposites. Cellulose 26 (8), 4827–4840.

Gustavsson, Lotta H., Adolfsson, Karin H., Hakkarainen, Minna, 2020. Thermoplastic "all-cellulose" composites with covalently attached carbonized cellulose. Biomacromolecules 21 (5), 1752–1761.

Hafrén, Jonas, Córdova, Armando, 2005. Direct organocatalytic polymerization from cellulose fibers. Macromol. Rapid Commun. 26 (2), 82–86.

Hafrén, Jonas, Córdova, Armando, 2007. Direct bronsted acid-catalyzed derivatization of cellulose with poly (l-lactic acid) and d-mandelic acid. Nord. Pulp Pap. Res. J. 22 (2), 184–187.

Ichiura, Hideaki, Hirose, Yuka, Masumoto, Misaki, Ohtani, Yoshito, 2017. Ionic liquid treatment for increasing the wet strength of cellulose paper. Cellulose 24 (8), 3469–3477.

Jamróz, Ewelina, Kulawik, Piotr, Kopel, Pavel, Balková, Radka, Hynek, David, Bytesnikova, Zuzana, Gagic, Milica, Milosavljevic, Vedran, Adam, Vojtech, 2019. Intelligent and active composite films based on furcellaran: structural characterization, antioxidant and antimicrobial activities. Food Packag. Shelf Life 22, 100405.

Jiang, Feng, Pan, Chenqian, Zhang, Yaqiong, Fang, Yanxiong, 2019. Cellulose graft copolymers toward strong thermoplastic elastomers via raft polymerization. Appl. Surf. Sci. 480, 162–171.

Kanmani, Paulraj, Rhim, Jong-Whan, 2014. Properties and characterization of bionanocomposite films prepared with various biopolymers and zno nanoparticles. Carbohydr. Polym. 106, 190–199.

Kaur, Harjinder, Rathore, Anuradha, Raju, Shinu, 2014. A study on zno nanoparticles catalyzed ring opening polymerization of l-lactide. J. Polym. Res. 21 (9), 1–10.

Koppolu, Rajesh, Lahti, Johanna, Abitbol, Tiffany, Swerin, Agne, Kuusipalo, Jurkka, Toivakka, Martti, 2019. Continuous processing of nanocellulose and polylactic acid into multilayer barrier coatings. ACS Appl. Mater. Interfaces 11 (12), 11920–11927.

Kosan, Birgit, Michels, Christoph, Meister, Frank, 2008. Dissolution and forming of cellulose with ionic liquids. Cellulose 15 (1), 59–66.

Leite, Monique J., Agner, Tamara, Machado, Fabricio, Neto, Brenno A.D., Araujo, Pedro H.H., Sayer, Claudia, 2022. ε-caprolactone ring-opening polymerization catalyzed by imidazolium-based ionic liquid under mild reaction conditions. J. Polym. Res. 29 (2), 1–8.

Liao, Liqiong, Liu, Lijian, Zhang, Chao, Gong, Shaoqin, 2006. Microwave-assisted ring-opening polymerization of ε-caprolactone in the presence of ionic liquid. Macromol. Rapid Commun. 27 (24), 2060–2064.

Liu, Hanbin, Sale, Kenneth L., Holmes, Bradley M., Simmons, Blake A., Singh, Seema, 2010. Understanding the interactions of cellulose with ionic liquids: a molecular dynamics study. J. Phys. Chem. B 114 (12), 4293–4301.

Lönnberg, Hanna, Fogelström, Linda, Zhou, Qi, Hult, Anders, Berglund, Lars, Malmström, Eva, 2011. Investigation of the graft length impact on the interfacial toughness in a cellulose/poly (ε-caprolactone) bilayer laminate. Compos. Sci. Technol. 71 (1), 9–12.

Lu, Pengbo, Cheng, Fan, Ou, Yanghao, Lin, Meiyan, Su, Lingfeng, Chen, Size, Yao, Xilang, Liu, Detao, 2017. Rapid fabrication of transparent film directly from wood fibers with microwave-assisted ionic liquids technology. Carbohydr. Polym. 174, 330–336.

Schmid Markus, Dallmann Kerstin, Bugnicourt Elodie, Cordoni Dario, Wild Florian, Andrea Lazzeri, and Noller Klaus.Properties of whey-protein-coated films and laminates as novel recyclable food packaging materials with excellent barrier properties.2012.

Mohammadi, Hamid, Kamkar, Abolfazl, Misaghi, Ali, 2018a. Nanocomposite films based on cmc, okra mucilage and zno nanoparticles: Physico mechanical and antibacterial properties. Carbohydr. Polym. 181, 351–357.

Mohammadi, Reza, Mohammadifar, Mohammad Amin, Rouhi, Milad, Kariminejad, Mohaddeseh, Mortazavian, Amir Mohammad, Sadeghi, Ehsan, Hasanvand, Sara, 2018b. Physico-mechanical and structural properties of eggshell membrane gelatin-chitosan blend edible films. Int. J. Biol. Macromol. 107, 406–412.

Mousa, Hamouda M., Abdal-Hay, Abdalla, Bartnikowski, Michal, Mohamed, Ibrahim M. A., Yasin, Ahmed S., Ivanovski, Saso, Park, Chan Hee, Kim, Cheol Sang, 2018. A multifunctional zinc oxide/poly (lactic acid) nanocomposite layer coated on magnesium alloys for controlled degradation and antibacterial function. ACS Biomater. Sci. Eng. 4 (6), 2169–2180.

Moyer, Preenaa, Smith, Micholas Dean, Abdoulmoumine, Nourredine, Chmely, Stephen C., Smith, Jeremy C., Petridis, Loukas, Labbé, Nicole, 2018. Relationship between lignocellulosic biomass dissolution and physicochemical properties of ionic liquids composed of 3-methylimidazolium cations and carboxylate anions. Phys. Chem. Chem. Phys. 20 (4), 2508–2516.

Niu, Xun, Liu, Yating, King, Alistair W.T., Hietala, Sami, Pan, Hui, Rojas, Orlando J., 2019. Plasticized cellulosic films by partial esterification and welding in low-concentration ionic liquid electrolyte. Biomacromolecules 20 (5), 2105–2114.

Noshirvani, Nooshin, Ghanbarzadeh, Babak, Mokarram, RezaRezaei, Hashemi, Mahdi, Coma, Véronique, 2017. Preparation and characterization of active emulsified films based on chitosan-carboxymethyl cellulose containing zinc oxide nano particles. Int. J. Biol. Macromol. 99, 530–538.

Pang, Jin Hui, Wu, Miao, Zhang, Qiao Hui, Tan, Xin, Xu, Feng, Zhang, Xue Ming, Sun, Run Cang, 2015. Comparison of physical properties of regenerated cellulose films fabricated with different cellulose feedstocks in ionic liquid. Carbohydr. Polym. 121, 71–78.

Priyadarshi, Ruchir, Kim, Se-Mi, Rhim, Jong-Whan, 2021. Carboxymethyl cellulose-based multifunctional film combined with zinc oxide nanoparticles and grape seed extract for the preservation of high-fat meat products. Sustain. Mater. Technol. 29, e00325.

Reis, Raquel Soares, de Holanda Saboya Souza, Diego, de Fátima Vieira Marques, Maria, Santos da Luz, Fernanda, Monteiro, Sergio Neves, 2021. Novel bionanocomposite of polycaprolactone reinforced with steam-exploded microfibrillated cellulose modified with zno. J. Mater. Res. Technol.

Reyes, Guillermo, Borghei, Maryam, King, Alistair W.T., Lahti, Johanna, Rojas, Orlando J., 2018. Solvent welding and imprinting cellulose nanofiber films using ionic liquids. Biomacromolecules 20 (1), 502–514.

Rezaei, Mohammad, Pirsa, Sajad, Chavoshizadeh, Sona, 2020. Photocatalytic/antimicrobial active film based on wheat gluten/zno nanoparticles. J. Inorg. Organomet. Polym. Mater. 30 (7), 2654–2665.

Rivera-Galletti, Ashley, Gough, Christopher R., Kaleem, Farhan, Burch, Michael, Ratcliffe, Chris, Lu, Ping, Salas-De la Cruz, David, Hu, Xiao, 2021. Silk-cellulose acetate biocomposite materials regenerated from ionic liquid. Polymers 13 (17), 2911.

Roy, Swarup, Rhim, Jong-Whan, 2020. Carboxymethyl cellulose-based antioxidant and antimicrobial active packaging film incorporated with curcumin and zinc oxide. Int. J. Biol. Macromol. 148, 666–676.

Roy, Swarup, Kim, Hyun Chan, Panicker, Pooja S., Rhim, Jong-Whan, Kim, Jaehwan, 2021. Cellulose nanofiber-based nanocomposite films reinforced with zinc oxide nanorods and grapefruit seed extract. Nanomaterials 11 (4), 877.

Rudnik, Ewa, 2013. Compostable polymer properties and packaging applications. Plastic Films in Food Packaging. Elsevier, pp. 217–248.

Saedi, Shahab, Shokri, Mastaneh, Kim, Jun Tae, Shin, Gye Hwa, 2021. Semi-transparent regenerated cellulose/znonp nanocomposite film as a potential antimicrobial food packaging material. J. Food Eng. 307, 110665.

Sand, Arpit, Yadav, Mithilesh, Behari, Kunj, 2010. Synthesis and characterization of alginate-g-vinyl sulfonic acid with a potassium peroxydiphosphate/thiourea system. J. Appl. Polym. Sci. 118 (6), 3685–3694.

Segal, L.G.J.M.A., Creely Jr, J., Martin Jr, A.E., Conrad, C.M., 1959. An empirical method for estimating the degree of crystallinity of native cellulose using the x-ray diffractometer. Text. Res. J. 29 (10), 786–794.

Shankar, Shiv, Wang, Long-Feng, Rhim, Jong-Whan, 2018. Incorporation of zinc oxide nanoparticles improved the mechanical, water vapor barrier, uv-light barrier, and antibacterial properties of pla-based nanocomposite films. Mater. Sci. Eng.: C 93, 289–298.

Siró, István, Plackett, David, 2010. Microfibrillated cellulose and new nanocomposite materials: a review. Cellulose 17 (3), 459–494.

Mariia Stepanova, Ilia Averianov, Iosif Gofman, Olga Solomakha, Yuliya Nashchekina, Viktor Korzhikov-Vlakh, and Evgenia Korzhikova-Vlakh.Poly (ε-caprolactone)-based biocomposites reinforced with nanocrystalline cellulose grafted with poly (l-lactic acid).In IOP Conference Series: Materials Science and Engineering, volume 500, page 012021. IOP Publishing, 2019.

Swatloski, Richard P., Spear, Scott K., Holbrey, John D., Rogers, Robin D., 2002. Dissolution of cellose with ionic liquids. J. Am. Chem. Soc. 124 (18), 4974–4975.

Terzopoulou, Zoi, Baciu, Diana, Gounari, Eleni, Steriotis, Theodore, Charalambopoulou, Georgia, Bikiaris, Dimitrios, 2018. Biocompatible nanobioglass reinforced poly (ε-caprolactone) composites synthesized via in situ ring opening polymerization. Polymers 10 (4), 381.

Valls, Cristina, Roncero, M. Blanca, 2013. Antioxidant property of tcf pulp with a high hexenuronic acid (hexa) content. Holzforschung 67 (3), 257–263.

Vannozzi, Lorenzo, Gouveia, Pedro, Pingue, Pasqualantonio, Canale, Claudio, Ricotti, Leonardo, 2020. Novel ultrathin films based on a blend of peg-b-pcl and plla and doped with zno nanoparticles. ACS Appl. Mater. Interfaces 12 (19), 21398–21410.

Villocillo, C.B., Angcajas, A.B., 2019. Biosorption of copper (ii) ions in aqueous solution by microwave-synthesized starch-graft-n-methyl-n-vinylacetamide. Biosci. Biotechnol. Res. Commun. 12, 211–221.

Vinogradova, Yevgeniya S., Chen, Jonathan Y., 2016. Micron-and nano-cellulose fiber regenerated from ionic liquids. J. Text. Inst. 107 (4), 472–476.

Wang, Jinwu, Gardner, Douglas J., Stark, Nicole M., Bousfield, Douglas W., Tajvidi, Mehdi, Cai, Zhiyong, 2018. Moisture and oxygen barrier properties of cellulose nanomaterial-based films. ACS Sustain. Chem. Eng. 6 (1), 49–70.

Wang, K.L., Jiang, N., He, B.B., Kang, D.X., 2017. Regiocontroll synthesis cellulose-graft-polycaprolactone copolymer (2, 3-di-o-pcl-cellulose) by a new route. Express Polym. Lett. 11 (12), 991–1002.

Wang, Zhaodong, Zheng, Liuchun, Li, Chuncheng, Zhang, Dong, Xiao, Yaonan, Guan, Guohu, Zhu, Wenxiang, 2013. A novel and simple procedure to synthesize chitosan-graft-polycaprolactone in an ionic liquid. Carbohydr. Polym. 94 (1), 505–510.

Wu, Hao, Nagarajan, S., Zhou, Lijuan, Duan, Yongxin, Zhang, Jianming, 2016. Synthesis and characterization of cellulose nanocrystal-graft-poly (d-lactide) and its nanocomposite with poly (l-lactide). Polymer 103, 365–375.

Wu, Juan, Sun, Qi, Huang, Hang, Duan, Ying, Xiao, Gang, Le, Tao, 2019. Enhanced physico-mechanical, barrier and antifungal properties of soy protein isolate film by incorporating both plant-sourced cinnamaldehyde and facile synthesized zinc oxide nanosheets. Colloids Surf. B: Biointerfaces 180, 31–38.

Xiao, Liqiang, Yao, Zheng, He, Yongbin, Han, Zeyu, Zhang, Xujing, Li, Chengcheng, Xu, Pengwu, Yang, Weijun, Ma, Piming, 2022. Antioxidant and antibacterial pbat/lignin-zno nanocomposite films for active food packaging. Ind. Crop. Prod. 187, 115515.

Xu, Airong, Wang, Yongxin, Liu, Rukuan, 2019. Cellulose dissolution in diallylimidazolium methoxyacetate+ n-methylpyrrolidinone mixture. Sci. Rep. 9 (1), 1–8.

Yousefi, Hossein, Mashkour, Mahdi, Yousefi, Razieh, 2015. Direct solvent nanowelding of cellulose fibers to make all-cellulose nanocomposite. Cellulose 22 (2), 1189–1200.

Yousefi, Hossein, Nishino, Takashi, Faezipour, Mehdi, Ebrahimi, Ghanbar, Shakeri, Alireza, 2011. Direct fabrication of all-cellulose nanocomposite from cellulose microfibers using ionic liquid-based nanowelding. Biomacromolecules 12 (11), 4080–4085.

Yu, Yongqi, Gao, Xin, Jiang, Zeming, Zhang, Wentao, Ma, Jiwei, Liu, Xuejiao, Zhang, Liping, 2018. Homogeneous grafting of cellulose with polycaprolactone using quaternary ammonium salt systems and its application for ultraviolet-shielding composite films. RSC Adv. 8 (20), 10865–10872.

Zhang, Di, Nie, Rong, Zhang, Chunyue, Wang, Yibing, Wang, Li, Chen, Tao, Zhao, Liming, 2022. Characterization of biodegradable food packaging films prepared with polyamide 4: Influence of molecular weight and environmental humidity. Food Bioeng.

Zhang, Jinming, Wu, Jin, Yu, Jian, Zhang, Xiaoyu, He, Jiasong, Zhang, Jun, 2017. Application of ionic liquids for dissolving cellulose and fabricating cellulose-based materials: state of the art and future trends. Mater. Chem. Front. 1 (7), 1273–1290.

Zhu, Linlin, Chen, Qinyong, Wang, Ying, Huang, Huishan, Luo, Wenyi, Li, Zhunxuan, Zhang, Zhen, Hadjichristidis, Nikos, 2021. Grafting polysulfonamide from cellulose paper through organocatalytic ring-opening polymerization of n-sulfonyl aziridines. Carbohydr. Polym. 261, 117903.

Zuppolini, Simona, Maya, IriczalliCruz, Diodato, Laura, Guarino, Vincenzo, Borriello, Anna, Ambrosio, Luigi, 2020. Self-associating cellulose-graft-poly (ε-caprolactone) to design nanoparticles for drug release. Mater. Sci. Eng.: C 108, 110385.